Pergamon

Acta Materialia 50 (2002) 1219–1227

Acta MATERIALIA

www.actamat-journals.com

An experimental study of the influence of imperfections on the buckling of compressed thin films

M.-W. Moon [a, d,*], J.-W. Chung [b], K.-R. Lee [b], K.H. Oh [a], R. Wang [c], A.G. Evans [d]

[a] *School of Material Science and Engineering, Seoul National University, Seoul 151-742, South Korea*
[b] *Future Technology Research Division, Korea Institute of Science and Technology, Seoul 130-650, South Korea*
[c] *Department of Metals and Materials Engineering, University of British Columbia, Vancouver, British Columbia, V6T 1R9 Canada*
[d] *Princeton Materials Institute, Princeton University, Princeton, NJ 08540, USA*

Received 28 September 2001; accepted 5 November 2001

Abstract

The role of imperfections on the initiation and propagation of buckle driven delaminations in compressed thin films has been demonstrated using experiments performed with diamond-like carbon (DLC) films deposited onto glass substrates. The surface topologies and interface separations have been characterized by using the Atomic Force Microscope (AFM) and the Focused Ion Beam (FIB) imaging system. The wavelengths and amplitudes of numerous imperfections have been measured by AFM and the interface separations characterized on cross sections made with the FIB. Chemical analysis of several sites, performed using Auger Electron Spectroscopy (AES), has revealed the origin of the imperfections. The incidence of buckles has been correlated with the imperfection wavelength. The findings have been rationalized in terms of theoretical results for the effect of imperfections on the energy release rate.

Keywords: Interface separation; Defect; Buckle driven delamination; Coating; FIB

1. Introduction

The responses exhibited by residually compressed thin films on thick substrates have been widely documented [1–7]. Most typically, in the presence of small interface separations, the films may buckle and, moreover, the buckles can propagate beneath the film if the induced energy release rate exceeds the interface fracture toughness. The ensuing buckles exhibit several configurations: ranging from circular to linear to telephone cord. Some examples from the present study are summarized in Fig. 1. The basic mechanics governing the propagation of the buckles, as well as their morphological tendencies, have been largely worked out and validated by experiment [2,7–14]. The initiation of the buckles has received much less attention. The focus of this article is on initiation.

As in all practical buckling problems, imperfections are expected to be important [6,15–21]. In

* Corresponding author.
E-mail address: mwmoon@princeton.edu (M.-W. Moon).

1359-6454/02/$22.00
PII: S1359-6454(01)00423-2

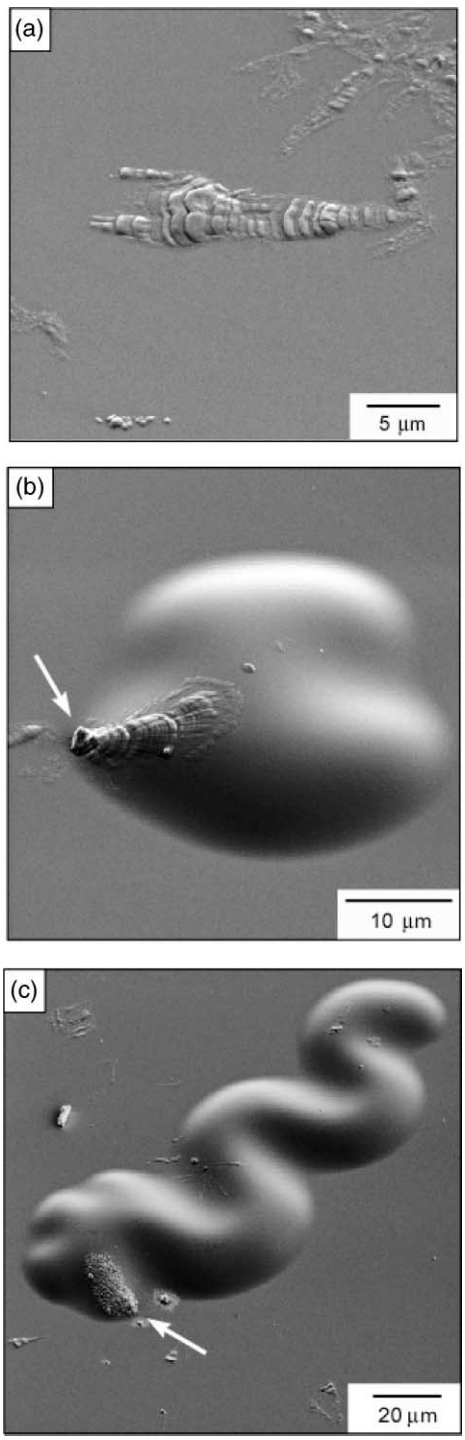

recognition of this, some effects of geometric imperfections have been recently analyzed [17–19]. The salient results for a surface protrusion are summarized in Fig. 2. Note that the energy release rate, G, for an interface separation beneath the imperfection is dramatically altered, relative to a flat surface. Most importantly, a finite G develops even for very small initial separations: attributed to the tensile stress normal to the interface [15,17]. Moreover, there is a minimum, $G_{\min}$, which arises for separations similar in diameter to the imperfection. This minimum is followed by a rapid increase, indicative of instability. The implication is that, if the minimum exceeds the fracture toughness of the interface, Γ_{int} (at the appropriate mode mixity [14]), the putative buckle becomes unstable and propagates beyond the imperfection: thereafter, assuming one of the configurations depicted in Fig. 1.

The specific objective of this article is to conduct an experimental study of imperfections for comparison with Fig. 2. For this purpose, a well-studied system has been chosen, consisting of thin films of diamond-like carbon (DLC) deposited onto nominally flat glass substrates. Such systems are typically subject to high residual compression (1–4 GPa) and modest adhesion, causing them to be susceptible to separation and buckling [22]. In order to characterize the imperfections, the precision of the atomic force microscope (AFM) and of the focused ion beam (FIB) imaging system has been exploited. Chemical analysis was executed with auger electron spectroscopy (AES).

2. Materials and characterization

The substrates consisted of standard microscope slides made from soda lime glass. The DLC films were deposited by using a capacitively coupled r.f. glow discharge, choosing conditions that generate telephone cord buckles [22]. The gas phases were CH_4 or C_6H_6 plus N_2, at a pressure of 1.33 Pa, and

Fig. 1. Three characteristic configurations. (a) An imperfection with no apparent buckle, (b) an imperfection (arrowed) at the perimeter of an axi-symmetric buckle and (c) an imperfection (arrowed) at one end of a telephone cord buckle.

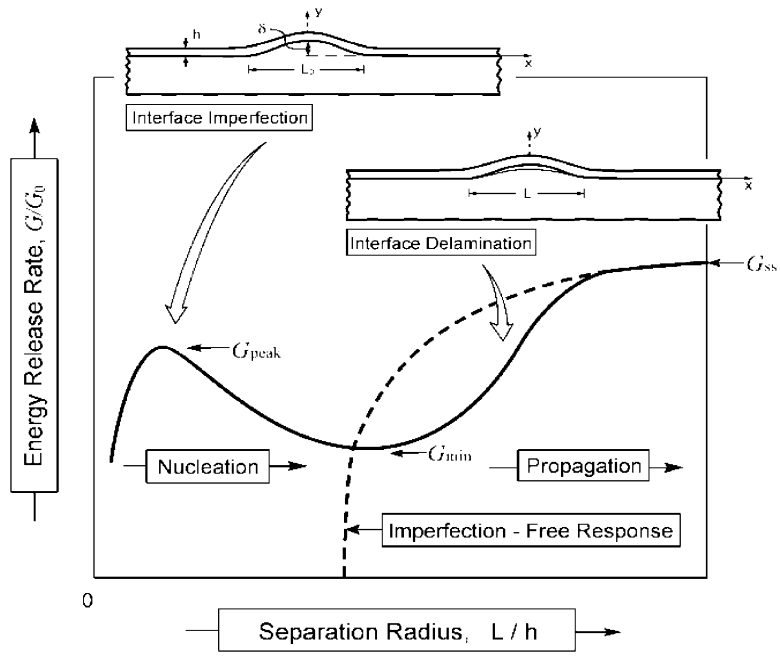

Fig. 2. The energy release rate as a function of separation diameter for thin compressed films on a surface with a protruding imperfection.

the deposition was performed at a negative self-bias voltage controlled in the range −100 to −700 V [5,22]. For these conditions, the film thickness was in the range 0.26 ~ 0.46 μm, and the residual compression between about 1 and 4 GPa [22], resulting in telephone cord buckles with wavelength about 20 ~ 25 μm. Various surface topologies appear (Figs. 1 and 3), indicative of a range of imperfections. It will be shown that these imperfections are all related to defects on the surface of the glass prior to DLC deposition.

The surfaces of the as-deposited materials were characterized by scanning electron microscopy (SEM) and atomic force microscopy (AFM). The AFM images were taken in tapping mode (Digital Instruments) at 2 nm resolution. The morphologies of the imperfections (and of the surrounding film) have been characterized by using the FIB imaging system. This system has the attribute that a small linear region passing through the buckle initiation site can be identified and a cross section made at that precise location, by means of a Ga ion beam, with minimal damage along the section plane. After sectioning, reconfiguring the instrument in the SEM mode enables imaging of the cross section. The specimen can also be removed from the FIB to conduct additional imaging and AFM characterization.

3. Observations and measurements

3.1. Surface profiles

Measurements have been performed on the imperfections shown in Fig. 1, as well as those in Fig. 3, beginning with the latter. The AFM surface profiles reveal four imperfection categories, having the amplitudes and wavelengths summarized in Table 1. The differing profiles suggest the three basic responses shown schematically in Fig. 3. These responses are validated below in the FIB cross sections. The two smaller imperfections (numbers I and II) both have amplitudes around 140 nm and wavelengths about 6.2 μm in diameter (Fig. 3(a) and (b)). Their irregular profiles indicate

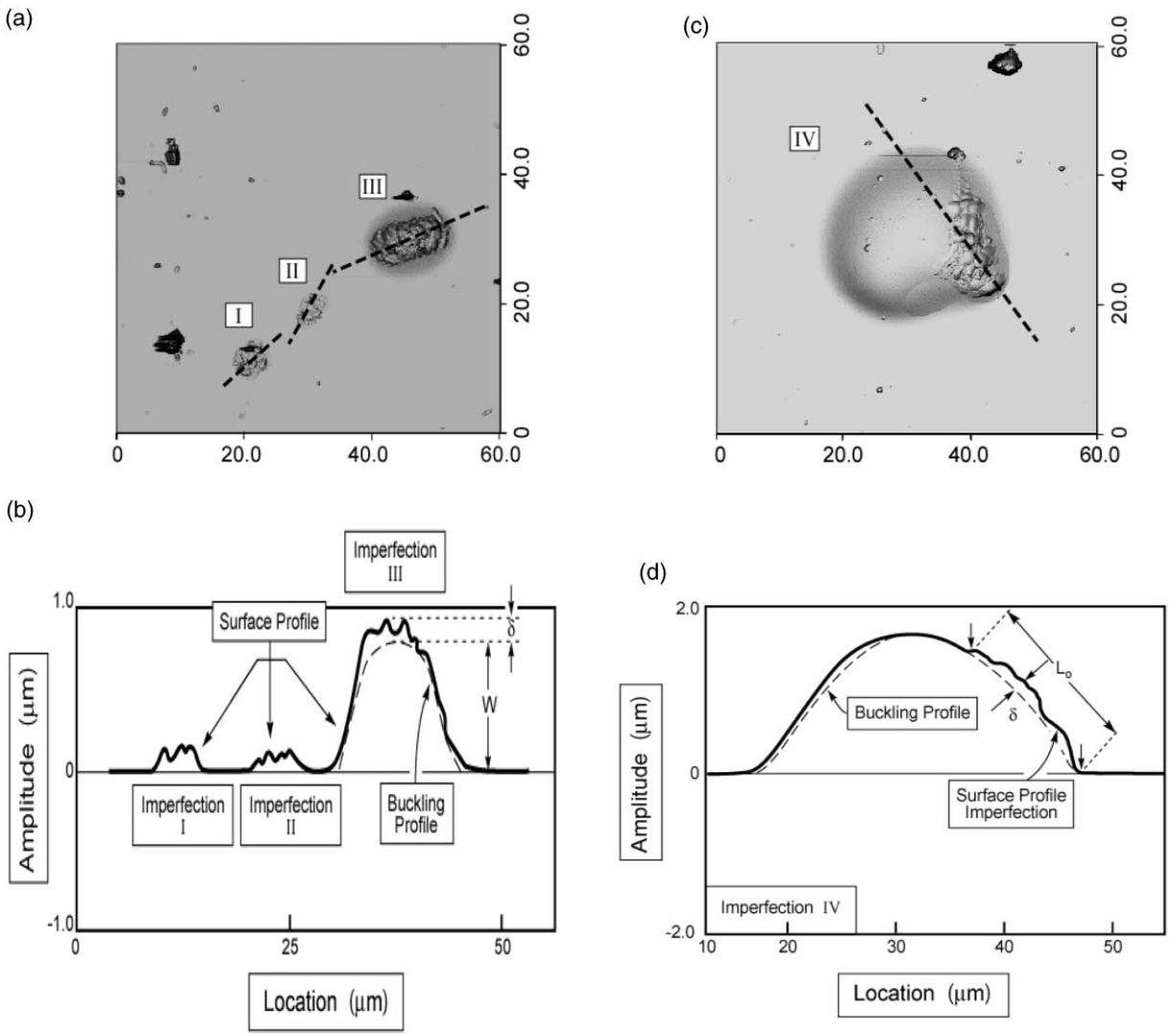

Fig. 3. SEM images and AFM surface profiles of four imperfections. (a) Images of three imperfections (I, II, III) showing the line sections used to measure the profiles. The largest imperfection (III) has contrast around the perimeter suggestive of a buckle. (b) The AFM profiles of imperfections I, II and III. The irregular profiles for I and II suggest an absence of buckling. The large amplitude of III and the smoother profile suggest an underlying buckle having the profile indicated by the dotted arc. The original imperfection amplitude and wavelength are estimated by subtracting the buckled arc from the surface profile. (c) Image of the largest imperfection (IV) indicative of an associated axi-symmetric buckle. (d) Surface profile of (c) and the underlying buckle profile, highlighting the original imperfection amplitude and wavelength.

that the DLC is still fully attached to the substrate. The somewhat larger imperfection (number III in Fig. 3(a)) has a substantially different profile. The irregular segment at the right (with features similar to imperfections I and II) appears to superpose on a smooth arc (Fig. 3(b)), suggestive of an interface that has separated and buckled. By constructing an arc that matches the profile on the left side, the deviation of the profile on the right, above the arc, provides an estimate of the size of the initial imperfection. This procedure indicates an imperfection amplitude $\delta = 230$ nm and wavelength, $L_0 =$

Table 1
The amplitude and wavelength of the 4 imperfections shown in Fig. 3

Imperfection	δ (nm)	L_o (μm)	L_o/h	δ/L_o
I	130	6.0	13.0	0.022
II	133	6.4	13.9	0.021
III	231	15.1	32.8	0.015
IV	360	20.0	43.5	0.018

15.1 μm. The profile of the arc indicates that the corresponding amplitude of the buckle is $w \approx 760$ nm. The largest imperfection (number IV in Fig. 3(c)) appears at the source of a propagating telephone cord buckle (Fig. 3(c) and (d)). By fitting an arc to the buckled region, as above, the imperfection size is determined to have amplitude $\delta =$ 360 nm and wavelength, $L_0 = 20.0$ μm (Table 1).

3.2. Cross sections

The FIB cross sections shown in Figs. 4 and 5 made on the imperfections shown in Fig. 1 appear to validate the assertions made above. In all cases, note that the irregular topology found on the surface reflects the initial topology of the substrate, affirming that the DLC deposits everywhere with uniform thickness, $h = 0.46$ μm. Images of a small imperfection that did not buckle (Fig. 4) confirm that the DLC remains attached to the substrate. The amplitude of the imperfection is smaller than the film thickness, $\delta = 0.6h$. Images of a larger imperfection that initiated a telephone cord buckle (Fig. 5) reveal the separation. The amplitude of this imperfection exceeds the film thickness, $\delta =$ $1.2h$. It is also asymmetric. Region "A" on the left has the larger wavelength, $L_1 \approx 60h$. This is also the side that dictates the direction in which the buckle propagates. In region "B" at the right, the imperfection wavelength is smaller, $L_2 = 18h$, and the buckle is stationary. Such asymmetry is typical.

3.3. Chemical analysis of imperfections

Chemical (AES) analysis of several imperfections on the glass substrate, conducted on sections where the DLC had been removed by spallation

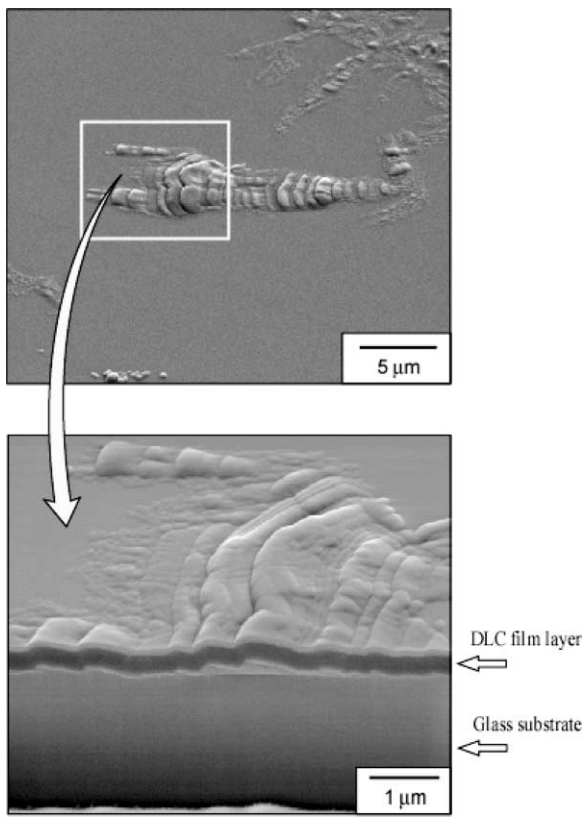

Fig. 4. One of the imperfections from Fig. 1(a), before and after cross sectioning with the FIB. Note that the film has uniform thickness such that the surface topography duplicates that for the substrate surface and that there is no separation at the interface.

(Fig. 6(a)) revealed the characteristics summarized in Fig. 6(b). In the smooth area I, only the components of silica (Si and O), were detected. In areas II and III associated with the imperfections, a major Ti peak is evident (around 400 eV) [23,24], suggestive of a Ti silicate phase, and another peak due to either Ca or C. The silicate is present as a contaminant that governs the size and shape of the surface imperfections on the glass.

3.4. Imperfection measurements

Measurements have been made on a large number of imperfections of the types described in the images. In each case, the imperfection amplitude and wavelength have been measured. The results

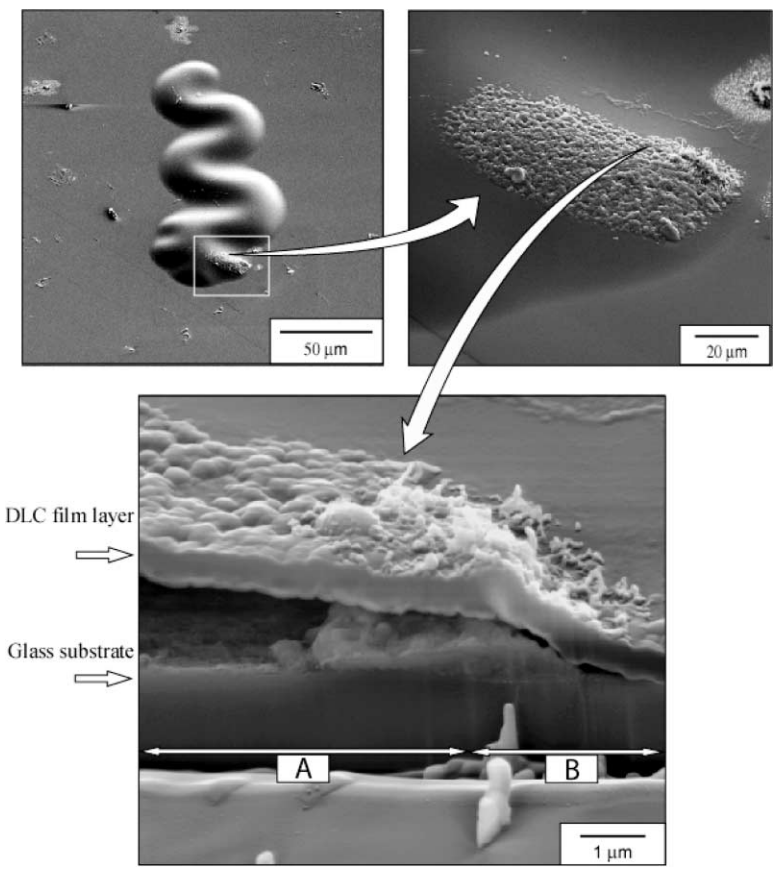

Fig. 5. Another imperfection from Fig. 1(c), before and after sectioning with the FIB, emphasizing the imperfection at one end of the telephone cord. Note that the DLC has uniform thickness and that a separation originates at the imperfection. The separation is asymmetric. Region "A" on the left has the larger wavelength, $L_1 \approx 60h$. This is also the side that dictates the direction in which the buckle propagates. In region "B" on the right, the imperfection wavelength is smaller, $L_2 = 18h$, and the buckle is stationary.

have been recorded in three categories. When the imperfections are strictly irregular, with profiles similar to either I/II in Fig. 3 or that in Fig. 4, the imperfection is classified as "sub-critical". When a well-defined telephone cord buckle has developed from the imperfection, as in Fig. 5, it is classified as "super-critical". All intermediate cases, where a buckle has formed but remains locally confined near the imperfection, are classified as "stationary". The results classified in this manner are plotted in Fig. 7, using δ/h and L/h as coordinates. Note that the super-critical imperfections cluster at larger values of L/h and the sub-critical imperfections at small L/h. This finding is rationalized below.

4. Analysis

The imperfections examined above are taken to be approximately axi-symmetric. The reference condition for axi-symmetric buckling of a thin residually compressed film on a flat surface, with interface separation, diameter L_b, is [14]:

$$L_b/h = 2.21\sqrt{\bar{E}/\sigma_R} \quad (1)$$

where $\bar{E}$ is the plane strain modulus of the film, $\bar{E} = E_{dlc}/(1-\nu^2)$, E_{dlc} is the Young's modulus and σ_R is the residual compression. When a protruding imperfection, amplitude d and wavelength L, is superposed on the flat surface, then the buckling resistance is negated, resulting in the energy

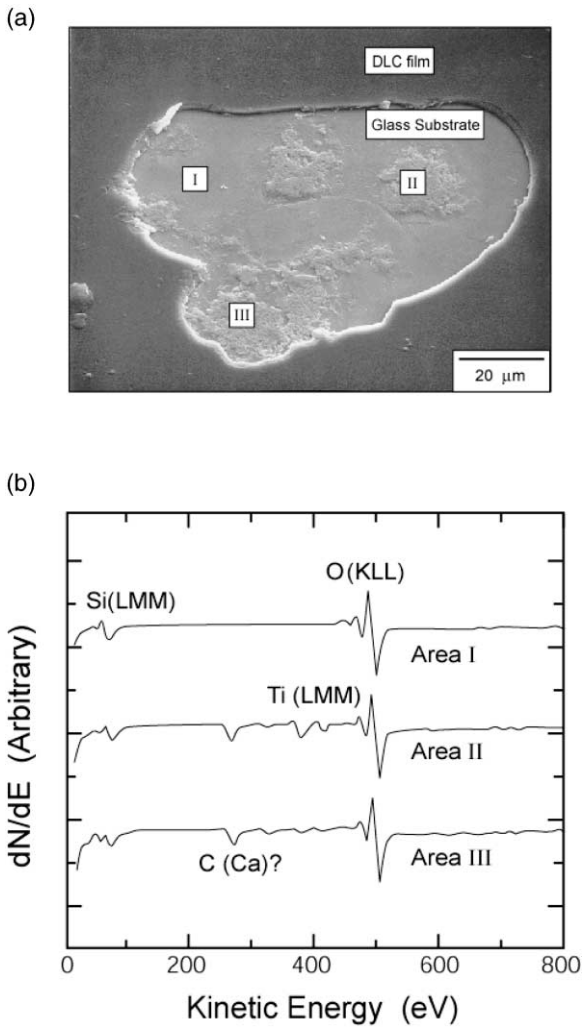

Fig. 6. Chemical analysis (AES) of the glass surface where the DLC film had been removed by spallation. (a) Image of glass surface showing planar areas (I) and imperfect areas (II and III). (b) AES spectra showing that in the planar areas only silicon and oxygen are detectable: whereas, at the imperfections, Ti is present as well as either C or Ca.

release rate depicted in Fig. 2. The minimum fits the analytic form [18]:

$$G_{\min}/G_{o} \approx 0.4(L/L_{b}) \tag{2}$$

where G_{o} is the delamination energy release rate [14]:

$$G_{o} = \frac{\sigma_{R}^{2} h}{2\bar{E}_{dlc}} \tag{3}$$

This result is insensitive to the amplitude of the imperfections within the range $0.05 \leq \delta/L \leq 0.2$ [18]. Analysis has yet to be performed outside this range. Noting that the imperfections summarized in Table 1 reside within this range (Fig. 7), Eq. (2) is used to rationalize the observations. For this purpose $G_{\min}$ is equated to the interface toughness, Γ_{int} at the appropriate mode mixity [14]. The consequence is a critical imperfection wavelength, L_{c}, above which a buckle forms and propagates into a telephone cord. It is given by:

$$\frac{L_{c}}{h} = 11\left(\frac{\Gamma_{int}}{\sigma_{R} h}\right)\left[\frac{\bar{E}}{\sigma_{R}}\right]^{3/2} \tag{4}$$

The critical wavelength determined from Eq. (4) can be superposed in Fig. 7 once the magnitudes of the parameters have been determined. The modulus is in the range $E = 90 \sim 100$ GPa [22]. The residual stress has been ascertained from the buckle wavelength as $\sigma_{R} = 1.9$ GPa [25]. The DLC thickness is $h = 0.46$ μm. The interface toughness is unknown, but is presumed to be less than that for the glass substrate, $\Gamma_{glass} = 8$ J m^{-2} [26]. Limits are ascertained by choosing values in the range $\Gamma_{int} = 4$ to 10 J m^{-2}. The transitions based on L_{c}/h are superposed in Fig. 7. They appear to separate the buckle propagation results. Imperfections that form telephone cord buckles occur in the super-critical domain, while those that resist buckling reside primarily in the sub-critical region. Further refinement requires that the interface toughness be measured at the relevant mode mixity [14].

5. Summary

A detailed experimental analysis has affirmed the effect of imperfections on the initiation of buckle-driven delaminations in compressed thin films. Diamond-like carbon films deposited onto nominally flat glass substrates were used for the investigation. Quantitative profiling by AFM characterized the amplitude and wavelength of imperfections. The FIB imaging system was used to characterize the imperfections on the substrate, at the buckle origination sites, as well as to establish the occurrence of inter-

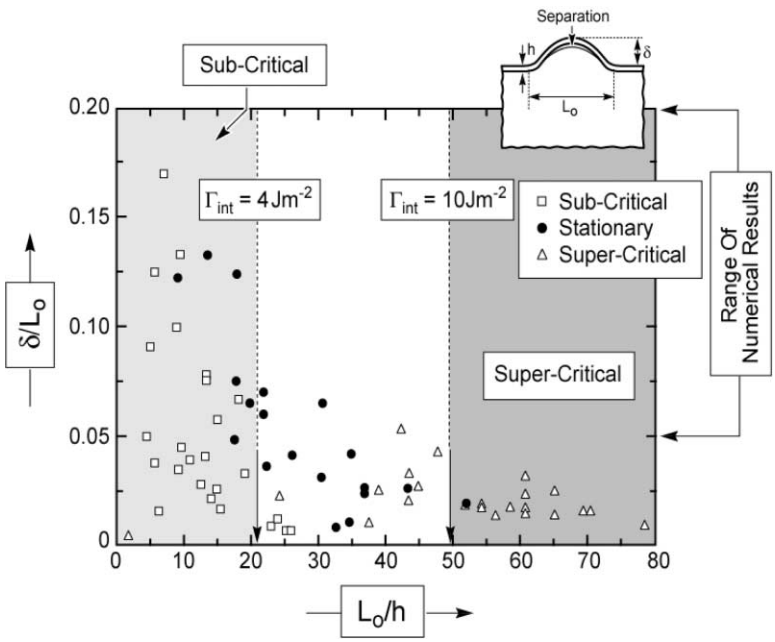

Fig. 7. Three categories for imperfection identified on a plot of aspect ratio δ/L and wavelength, L/h. When the imperfections are irregular with no interface separation, they are classified as "sub-critical". When they are at the origin of a well-defined telephone cord buckle they are classified as "super-critical". All intermediate cases, where a buckle has formed but remains locally confined near the imperfection, are classified as "stationary".

face separations and to affirm the film thickness. Measurements of this type, made on a large number of imperfections, have been rationalized in terms of the energy release rate at the onset of instability, which classifies the imperfections as; sub-critical, stationary, and super-critical. It has been shown that imperfections initiating telephone cord buckles are consistent with the super-critical domain and that those resistant to buckling reside within the sub-critical domain.

Acknowledgements

The authors would like to acknowledge helpful discussions with Professor J.W. Hutchinson in Harvard University.

References

[1] Matuda N, Baba S, Kinbara A. Thin Solid Films 1981;81:301.
[2] Evans AG, Hutchinson JW. Int J Solids Struct 1984;20:455.
[3] Nir D. Thin Solid Films 1984;112:41.
[4] Gille G, Rau B. Thin Solids Films 1984;120:109.
[5] Lee K-R, Baik Y-J, Eun K-Y. Diamond Relat Mater 1993;2:218.
[6] Tolpygo VK, Clarke DR. Mater Sci Eng 2000;A278:151.
[7] Jensen HM, Hutchinson JW, Kim K-S. Int J Solids Struct 1990;26:1099.
[8] Chai H, Babcock CD, Knauss WG. Int J Solids Struct 1981;11:1069.
[9] Kublanov LB, Bottega WJ. Appl Math Modelling 1995;19:499.
[10] Thouless MD, Hutchinson JW, Liniger EG. Acta Metal Mater 1992;40:2639.
[11] Colin J, Cleymand F, Coupeau C, Grilhe J. Phil Mag A 2000;80:2559.

[12] Hutchinson JW, Thouless MD, Liniger EG. Acta Metal Mater 1992;40:295.
[13] Wang J-S, Evans AG. Acta Mater 1998;46:4993.
[14] Hutchinson JW, Suo Z. Adv Appl Mech 1992;29:63.
[15] He MY, Evans AG, Hutchinson JW. Mater Sci Eng 1998;A245:168.
[16] Mumm DR, Evans AG. Acta Mater 2000;48:1815.
[17] Evans AG, Hutchinson JW, He MY. Acta Mater 1999;47:1513.
[18] Hutchinson JW, He MY, Evans AG. J Mech Phys Solids 2000;48:709.
[19] Wang J-S, Evans AG. Acta Mater 1999;47:699.
[20] Evans AG, He MY, Hutchinson JW. Acta Mater 1997;45:3543.
[21] Ito YM, Rosenblatt M, Cheng LY, Lange FF, Evans AG. Int J Fract 1981;17:483.
[22] Cho S-J, Lee K-R, Eun KY, Hahn JH, Ko D-H. Thin Solid Films 1999;341:207.
[23] Solomon JS, Baun WL. Surf Sci 1975;51:228.
[24] Tuan A, Yoon M, Medvedev V, Ono Y, Ma Y, Rogers Jr. JW. Thin Solid Films 2000;377-378:766.
[25] Moon M-W, Jenson HM, Hutchinson JW, Oh KH, Evans AG, to be published.
[26] Weiderhorn SM. J Am Ceram Soc 1967;50:407.